INTERNATIONAL JOURNAL FOR NUMERICAL METHODS IN FLUIDS, VOL. 18, 953–981 (1994)

ANALYSIS OF PERIODIC 3D VISCOUS FLOWS USING A QUADRATIC DISCRETE GALERKIN BOUNDARY ELEMENT METHOD

CHIU Y. CHAN,*‡ ANTONY N. BERIS*‖ AND SURESH G. ADVANI†

*Department of Chemical Engineering, †Department of Mechanical Engineering, Center for Composite Materials, University of Delaware, Newark, DE 19716, U.S.A.

SUMMARY

A discrete Galerkin boundary element technique with a quadratic approximation of the variables was developed to simulate the three-dimensional (3D) viscous flow established in periodic assemblages of particles in suspensions and within a periodic porous medium. The Batchelor's unit-cell approach is used. The Galerkin formulation effectively handles the discontinuity in the traction arising in flow boundaries with edges or corners, such as the unit cell in this case. For an ellipsoidal dilute suspension over the range of aspect ratio studied (1 to 54), the numerical solutions of the rotational velocity of the particles and the viscosity correction were found to agree with the analytic values within 0·2% and 2% respectively, even with coarse meshes. In a suspension of cylindrical particles the calculated period of rotation agreed with the experimental data. However, Burgers' predictions for the correction to the suspension viscosity were found to be 30% too low and therefore the concept of the equivalent ellipsoidal ratio is judged to be inadequate. For pressure-driven flow through a fixed bed of fibres, the prediction on the permeability was shown to deviate by as much as 10% from the value calculated based on approximate permeability additivity rules using the corresponding values for planar flow past a periodic array of parallel cylinders. These applications show the versatility of the technique for studying viscous flows in complicated 3D geometries.

KEY WORDS Galerkin bounday element method Unit-cell approach Traction discontinuities Suspension rheology High fibre aspect ratio flow through a porous medium

INTRODUCTION

Since the pioneering work of Youngren and Acrivos,[1] the use of the boundary element method (BEM) in the approximation of multidimensional Stokes flow has increased greatly, as demonstrated by the plethora of articles that have appeared in the literature on this subject—for example, see the two recent textbooks by Kim and Karrila[2] and Pozrikidis[3] and references cited therein. The interest in the BEM stems from the reduction of the dimensionality of the problem accomplished through the use of a boundary integral formulation which leads to reduced CPU and storage requirements. This algorithmic development in the solution of multidimensional Stokes equations, in conjunction with the use of faster and bigger computers, recently allowed the evaluation of the flow field within geometries of such complexity as, for example, encountered in the flows of multiparticle systems,[4–6] extrusion[7] and mixing[8] applications.

‡ Present address: ARCO Chemicals, Newtown Square, PA 19703, U.S.A.
‖ Author to whom correspondence should be addressed.

CCC 0271–2091/94/100953–29 *Received October 1993*

Solving Stokes flow problems is only one of the many applications of the BEM in the solution of systems of linear partial differential equations (PDEs). The general theory of the BEM can be found in several texts.[9–11] In the last 15 years the BEM has become the method of choice for a variety of problems involving complex domain boundaries, ranging from electrostatics to elasticity and viscous flows. Despite this, the mathematical theory of BEM approximations still lags compared with the more classical approaches represented by the finite differerence and finite element methods. Indeed, a general theory of error estimation for three-dimensional (3D) collocation BEM approximations is still lacking.[11] Even for two-dimensional (2D) problems no collocation convergence results are available for problems involving domains with corners, mixed boundary value problems or boundary integral equations of different orders.[11] Only the theory of convergence and error estimates for the Galerkin BEM is well developed,[12–16] but even there the question of whether the convergence can be observed in practice, especially with integral equations of the first kind which result in linear equations with a high condition number, is still unresolved.[17,18]

Of particular interest to the numerical analyst is the understanding of how in practice the various factors affecting the numerical error (such as the numerical approximation of the surface, the nature of the basis functions, the numerical evaluation of the integrals, etc.) influence the convergence characteristics. Numerical experiments aiming to demonstrate the convergence characteristics of the BEM are the only means to demonstrate in practice the performance of this computational technique. Given the limited availability of computational resources, this information is crucial in order to select the optimum values for the numerical parameters which determine the distribution of the workload among the two principal computational tasks: the numerical integration and the solution of linear equations.

The task of optimizing the numerical implementation of the BEM becomes difficult if one considers the fact that there is (in general) more than one possible boundary integral representation for any given problem and that for each such representation there are several numerical formulations. The boundary integral formulations are primarily characterized by the nature of the resulting Fredholm integral equations, which are of the first or second kind. The integral equations of the second kind are numerically stable and hence tend to be preferred in engineering applications. However, in this formulation all the essential properties of the original elliptical operators such as symmetry, coerciveness and variational form are generally not preserved.[19] Since these properties help establish the existence and uniqueness of the exact solution, it may be particularly important to preserve these properties in cases where compatibility with the more traditional techniques, such as finite elements of the corresponding elliptical operators, is sought.[18] On the other hand, it is a well-known fact that Fredholm equations of the first kind are poorly conditioned, i.e. the solution usually leads to a system of linear equations with high condition numbers, especially when a large number of elements are used. However, as can be shown (analytically in certain situations[18] and numerically in others[20]), this deficiency does not necessarily prohibit the attainment of good accuracy with finite size discretizations with the integral equations of the first kind.

More specifically, for the 3D Stokes problem the Green function approach leads to Fredholm integral equations of the first kind (when velocity values are prescribed along the system boundary), whereas the double-layer potential approach results in Fredholm integral equations of the second kind. In this paper the focus is only on the first approach, which is amenable to the use of engineering quantities such as the velocities and the tractions as the primary variables.[1] The interested reader is referred to two recent texts for additional information on the second approach.[2,3] Although we hope that the conclusions from our investigations can also be of relevance to other BEM applications corresponding to other formulations or even different

problems, the present work focuses, for practical reasons, on the investigation of a special issue. This is the numerical implementation of the piecewise Lagrangian interpolation of the Green function solution to the 3D Stokes flow.

The goal of the present work was to implement a second-order discontinuous polynomial approximation to the Galerkin boundary element formulation for 3D viscous (Stokes) flow confined by non-smooth boundaries. Such problems arise frequently in engineering practice. Non-smooth boundaries such as corners and edges are not only encountered in flows around blunt objects (such as cubes, cylindrical particles of finite aspect ratio, etc.) but also when periodic flow problems are simulated through the use of the unit-cell technique.[21,22] So far, only low-order collocation boundary element (constant element) formulations have been used to approximate 3D periodic viscous flows,[22] necessitating a large number of unknowns to obtain accurate results. The need to expand the user of higher-order approximations to such problems was the motivation behind the present work.

A barrier towards the efficient numerical implementation of a high-order Galerkin boundary element method to problems involving discontinuous tractions at the boundaries, such as those encountered in domains involving corners, has been the accurate numerical evaluation of nearly singular integrals. These are the type of integrals encountered in the boundary integral formulation of the Stokes equations for points of reference which lie close to but out of the plane of the element under consideration. Their accurate and efficient numerical evaluation is crucial for the convergence of the BEM. The enabling technique to achieve this task, relying on an adaptive evaluation technique through domain subdivision, has been recently developed in our previous paper.[20] A second-order collocation boundary element technique has been successfully tested in the evaluation of the flow field around spherical and ellipsoidal particles at close proximity (at distances down to 0·01% of the particle diameter). The same technique of numerical integration is used in the present work in order to implement a discrete Galerkin formulation of the boundary element approximation of flows within or around domains involving edges and corners.

The (continuous) Galerkin approach has seldom been used since it requires the analytical evaluation of complex integral expressions which are only available for a very limited class of equations, surfaces (2D) and numerical approximations. However, recent theoretical developments have shown that the necessary integrals can be evaluated numerically with no loss in accuracy, at least for a range of smooth 2D problems.[14,23] Indeed, for specific kernerls the numerical integration rules can be sufficiently well tuned to lead to an even higher order of convergence (superconvergence) than the corresponding continuous Galerkin approach.[24] The corresponding methods can be distinguished based on how the integrals are evaluated: in discrete Galerkin the integrals are evaluated through the use of Gaussian quadrature;[14] in Galerkin collocation the lower-continuity finite element trial functions are used;[23] in qualocation a special weighting and specific collocation points are used.[24] Among those techniques the most general one (and the one employed in this work) is the discrete Galerkin.

The discrete Galerkin technique, similar to the (continuous) Galerkin technique, has not been used often in engineering applications,[3,25] primarily because of its increased computational requirements as compared with the collocation technique. The high computational requirements arise because the Galerkin approach requires an additional integration of the governing equations, as opposed to the collocation method where the governing equations are simply evaluated at the nodal points. When this additional integration is implemented numerically through a Gauss quadrature, it necessitates the evaluation of the boundary integral equations at more points, as compared with the nodal locations. This translates into an increased computational load for the construction of the governing equations. However, as parallel

computers become more established as the new computational environment, this drawback of Galerkin techniques will be partially alleviated and the higher accuracy of the Galerkin method will become more attractive. Since the numerical integration can be parallelized effortlessly with 100% efficiency,[26] the less efficiently parallelized solution of linear equations through LU decomposition will become more important in determining the computational requirements of the method.

The major motivation for the use of a Galerkin approach in the present work is the natural capability it offers in the handling of discontinuities in the variables, in particular those encountered in the tractions induced by a discontinuous change in the normal vectors around edges and corners. For flows involving boundaries with geometrical discontinuities, the accuracy of the BEM collocation computations generally declines, though reportedly only at the local level.[3] In a recent book by Pozrikidis[3] it is noted that: 'Higdon[27] and Pozrikidis[28] found that that the presence of sharp corners neither decrases the global accuracy nor discredits the overall liability of boundary element computations. On the other hand, Kelmanson[29,30] found that discontinuous boundary velocities might cause oscillatory solutions and slow convergence'. One way to avoid excessive error is through adaptive mesh refinement, though this is not always a cure for the problem.[29,30] Another way is that whenever the singular part is known, subtract it from the solution.[3] However, these asymptotic solutions are seldom available and are primarily restricted to 2D flows.[3]

The presence of a boundary discontinuity (corner or edge) frequently causes the main problem, which is the discontinuity in the fluxes at those locations due to the discontinuous change in the direction of the normal vector. Traditionally, corners are handled within a collocation implementation of the boundary element method by shifting the nodal points from the edges of the adjacent to the corner elements, thus allowing the fluxes to be discontinuous at the corner.[2] Although this approach is found to work satisfactorily, its numerical implementation is quite restrictive since it does not permit uniform mesh refinement (see discussion below). On the other hand, the handling of corner or edge singularities within the context of a Galerkin approach is straightforward and naturally follows the general rule of the method, which is simply extended to a discontinuous representation of the variables at the corner or edge under consideration. As long as no derivatives of the variables in question are involved in the formulation, which is duly satisfied in the case of the BEM, the Galerkin weighted residual equations can be formed equally well whether or not there is discontinuity. This is the approach followed here, thus opening new possibilities for the application of BEM techniques in flows through a porous medium, suspension rheology and in general areas where periodicity is assumed and the resulting calculations are based on a unit-cell approach involving corners by necessity.

The examples presented in this work involve corners or geometric discontinuities encountered in composite materials processing flows. Two types of problems are solved. The first one deals with a suspension of ellipsoids where the ellipsoids may move and rotate when the Newtonian fluid flows across them. Usually the orientation state and the rheological properties of such flowing suspensions are of interest and are continuously changing. We calculated these variables of interest using the developed BEM method. The second problem is presented to emphasize the versatility of the method and to exhibit the potential in handling intrinsically complex surfaces, e.g. flow through a fixed bed of fibres. Here the fibres are continuous, form a fixed network and may contain many geometric discontinuities. The pressure-driven flow through a porous medium is solved and the permeability of the medium is evaluated. Some of the results are compared with available analytic solutions to verify the numerical solution, while other results reveal the shortcomings of the assumptions made in order to simplify the equations in the quest to obtain a closed-form solution.

Next we discuss the important features of the numerical formulation, such as integral evaluation and the handling of corners and edges, and describe previous failed collocation attempts and the current successful approach. The section of results tabulates the convergence studies in smooth problems of two spheres where the analytic solution is available. Then the results and discussion for flow of dilute suspensions and flow across a periodic porous medium are presented.

FORMULATION

Stokes flow

The Stokes flow over a domain Ω past an arbitrary particle with surface Γ is described by

$$\nabla \cdot \mathbf{u} = 0, \qquad \mathbf{0} = -\nabla p + \mu \nabla^2 \mathbf{u}, \tag{1}$$

where $\mathbf{u}$ is the velocity vector, p is the pressure and μ is the viscosity. Note that only the pressure and viscous terms are retained in the momentum equations. As shown in Figure 1, there are in general two boundary conditions,

$$\mathbf{u} = \bar{\mathbf{u}} \quad \text{on } \Gamma_1, \qquad \mathbf{q} = \bar{\mathbf{q}} \quad \text{on } \Gamma_2, \tag{2}$$

where $\mathbf{q} = \boldsymbol{\sigma} \cdot \mathbf{n}$ is the traction on the particle surface, $\boldsymbol{\sigma}$ is the stress tensor and $\mathbf{n}$ is the outward normal.

The solution to the Stokes problem can be reduced to the solution of a set of integral equations[2]

$$c(\mathbf{y})u_i(\mathbf{y}) = \int_\Gamma u^*_{ij}(\mathbf{y}, \mathbf{z}) q_j(\mathbf{z})\, d\Gamma_z + \int_\Gamma \sigma^*_{ijk}(\mathbf{y}, \mathbf{z}) n_k(\mathbf{z}) u_j(\mathbf{z})\, d\Gamma_z, \tag{3}$$

where

$$c(\mathbf{y}) = \begin{cases} -1{\cdot}0 & \text{if point } \mathbf{y} \text{ is inside } \Omega, \\ -0{\cdot}5 & \text{if point } \mathbf{y} \text{ is on } \Gamma, \\ 0{\cdot}0 & \text{if point } \mathbf{y} \text{ is outside } \Omega \end{cases}$$

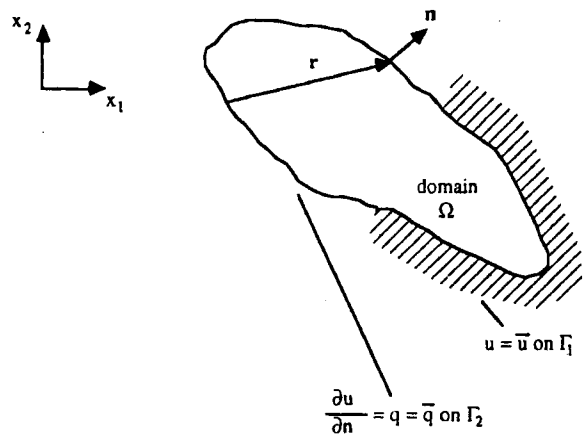

Figure 1. Boundary conditions in the boundary integral method

for a smooth boundary and where Einstein's implicit summation notation over repeated indices is used. The functions u_{ij}^* and σ_{ijk}^* are the fundamental solution to equation (3) and for flow in an unbounded domain are given by[31]

$$u_{ij}^*(\mathbf{y}, \mathbf{z}) = -\frac{1}{8\pi}\left(\frac{\delta_{ij}}{r} + \frac{r_i r_j}{r^3}\right), \tag{4}$$

$$\sigma_{ijk}^*(\mathbf{y}, \mathbf{z}) = \frac{1}{8\pi}\frac{6 r_i r_j r_k}{r^5}, \tag{5}$$

where $r^2 = \mathbf{r} \cdot \mathbf{r}$ and $\mathbf{r}(\mathbf{y}, \mathbf{z}) = \mathbf{z} - \mathbf{y}$. Physically u_{ij}^* represents the ith component of velocity at point $\mathbf{z}$ due to a point force in the j-direction applied at point $\mathbf{y}$.

In the BEM the functions $\mathbf{u}$ and $\mathbf{q}$ are discretized and expressed as linear combinations of the interpolation functions φ_k, weighted by the nodal values:

$$\mathbf{u}(\xi) = \sum_{k=1}^{m} \varphi_k \mathbf{u}_k, \tag{6}$$

$$\mathbf{q}(\xi) = \sum_{k=1}^{m} \varphi_k \mathbf{q}_k, \tag{7}$$

where φ_k is a piecewise continuous interpolation function and m depends on the order of the interpolation function and the type of element used (quadrilateral or triangular). In general the interpolation function can be zeroth-order (constant), first-order (linear), second-order (quadratic) or higher-order. The higher-order functions approximate the curvature of the variables better, thus improving the accuracy.[32] Similarly the domain geometry can be approximated as

$$\mathbf{x}(\xi) = \sum_{k=1}^{m} \Theta_k \mathbf{x}_k, \tag{8}$$

where Θ_k is also a piecewise continuous interpolation function. If φ and Θ are of the same order, the discretization is said to be 'isoparametric'. Although an isoparametric discretization has been used in the present work, we found higher accuracy using a superparametric (order of $\theta > \varphi$) discretization.[20]

In the collocation BEM the unknown nodal values are evaluated by solving a set of linear equations generated by writing equation (3) at each point. At the ith nodal point equation (3) in discretized form becomes

$$cu_i = \sum_{n=1}^{N} \int_{\Gamma_n} q_j u_{ij}^* \, d\Gamma + \sum_{n=1}^{N} \int_{\Gamma_n} \sigma_{ijk}^* n_k u_j \, d\Gamma, \tag{9}$$

where N is the total number of elements in the problem. Equation (9) can be rearranged in the form

$$\mathbf{H}\mathbf{u}^{\mathrm{G}} = \mathbf{G}\mathbf{q}^{\mathrm{G}}, \tag{10}$$

where $\mathbf{H}$ and $\mathbf{G}$ are $3M \times 3M$ influence matrices and $\mathbf{u}^{\mathrm{G}}$ and $\mathbf{q}^{\mathrm{G}}$ are the global velocity and traction vectors of size $3M$. M is the total number of nodes. Note that $\mathbf{H}$ and $\mathbf{G}$ depend only on the particle geometry and not on the boundary conditions.

The unit-cell approach

Batchelor[21] showed that the particle extras stress, or the stress contributed by the particles, within a volume V is given by

$$\sigma_{ij}^{(p)} = \frac{1}{V} \sum_{\alpha}^{N_p} \int_{\Gamma} [\sigma_{ik}(x_j - x_{cj})^{\alpha} n_k - \mu(u_i n_j + u_j n_i)] \, d\Gamma, \tag{11}$$

where the integral is taken over the surface Γ of each particle α and the summation is over all N_p particles in the volume. The fluid is considered to be statistically homogeneous and $\sigma_{ik} n_k$ is the force per unit area acting on the particle surface by the surrounding fluid. The vector $\mathbf{x} - \mathbf{x}_c$ denotes the positional vector of a point on the surface measured from $\mathbf{x}_c$, the centroid of the particle.

The term 'unit-cell approach' is not new—it has been referenced in the early editions of the classic book by Happel and Brenner.[33] For a periodic suspension equation (11) can be simplified by noting that the second term in square brackets cancels out. Thus

$$\sigma_{ij}^{(p)} = \frac{1}{V} \sum_{\alpha}^{N_p} \int_{\Gamma} \sigma_{ik}(x_j - x_{cj})^{\alpha} n_k \, d\Gamma, \tag{12}$$

where V is the unit cell described in equation (11). Equation (12) was used in postprocessing to evaluate the particle extra stress.

The unit-cell formalism is extremely powerful since it reduces a numerical problem containing thousands of particles to one containing only a few particles as shown in Figure 2. Using Batchelor's unit-cell model, the rheology of a suspension can be determined from the stress distribution on the particle surface. If the stress on a set of particles in a given configuration of the particles and for an imposed flow field is determined, the rheology of such a suspension can be found readily through the use of equation (12). However, it is important to remember the

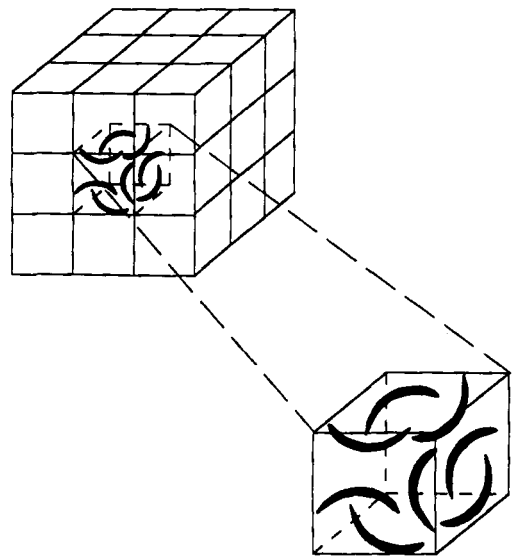

Figure 2. Simulation of an infinite suspension of fibers using an array of identical unit cells

assumption that the configuration used is representative of the actual particle configurations encountered during the flow. The properly evaluated stresses should involve taking an ensemble average, i.e. an average over all the different configurations weighted by the probability of their occurrence. Hence, the choice of the particle configuration is critical and a knowledge (or a model) of the configuration distribution is needed. The volume V should contain a representative sample of the particles such that the variation in local statistical properties of the suspension over V is negligible.

A unit cell is assumed to be periodically repeated in all three directions. For simple shear flow the periodic boundary conditions are similar to those used by Tran-Cong *et al.*,[5] except that in this study periodicity is prescribed in all directions. Consider a unit cell with dimensions $2L_1 \times 2L_2 \times 2L_3$ with the origin placed at the centroid of the cell:

$$\begin{aligned} \mathbf{u}(-L_1, x_2, x_3) &= \mathbf{u}(L_1, x_2, x_3), & \sigma(-L_1, x_2, x_3) &= \sigma(L_1, x_2, x_3), \\ \mathbf{u}(x_1, -L_2, x_3) &= \mathbf{u}(x_1, L_2, x_3), & \sigma(x_1, -L_2, x_3) &= \sigma(x_1, L_2, x_3), \\ \mathbf{u}(x_1, x_2, -L_3) &= \mathbf{u}(x_1, x_2, L_3), & \sigma(x_1, x_2, -L_3) &= \sigma(x_1, x_2, L_3) \end{aligned} \tag{13}$$

To impose shear flow, the velocities are prescribed only at the corners of the unit cell:

$$\mathbf{u}(\pm L_1, \pm L_2, L_3) = \mathbf{U}(L_3), \qquad \mathbf{u}(\pm L_1, \pm L_2, -L_3) = \mathbf{U}(-L_3). \tag{14}$$

Since $\mathbf{q} = \boldsymbol{\sigma} \cdot \mathbf{n}$ and the surfaces within each pair of periodic surfaces have opposite directions of $\mathbf{n}$, periodicity implies that the tractions will be opposite in directions:

$$\begin{aligned} \mathbf{q}(-L_1, x_2, x_3) &= -\mathbf{q}(L_1, x_2, x_3), & \mathbf{q}(x_1, -L_2, x_3) &= -\mathbf{q}(x_1, L_2, x_3), \\ & & \mathbf{q}(x_1, x_2, -L_3) &= -\mathbf{q}(x_1, x_2, L_3). \end{aligned} \tag{15}$$

At any node on a surface where periodicity applies, say (L_1, x_2, x_3), neither $\mathbf{u}$ nor $\mathbf{q}$ is known. Thus there are three equations generated from the integral equation at this node but there are six unknowns (three components of $\mathbf{u}$ and three of $\mathbf{q}$). The same can be said about its periodic node partner at $(-L_1, x_2, x_3)$. The six extra equations required to remove this indeterminancy are provided by the boundary conditions: the three $\mathbf{u}$-equations in (13) and the three $\mathbf{q}$-equations in (15).

For Poiseuille flow the handling of the periodic boundary conditions is similar. Only the periodic boundary condition for the stress in the direction of the pressure drop needs to be modified. We chose x_1 as the direction for pressure drop and flow; hence the only boundary condition that will be different from equation (13) is

$$\sigma(-L_1, x_2, x_3) - \sigma(L_1, x_2, x_3) = (\Delta p, 0, 0)^{\mathrm{T}}, \tag{16}$$

where $\Delta p = p|_{x_1 = L_1} - p|_{x_1 = -L_1}$. In this case the tractions will be given by

$$\begin{aligned} \mathbf{q}(-L_1, x_2, x_3) + \mathbf{q}(L_1, x_2, x_3) &= (-\Delta p, 0, 0)^{\mathrm{T}}, \\ \mathbf{q}(x_1, -L_2, x_3) = -\mathbf{q}(x_1, L_2, x_3), &\qquad \mathbf{q}(x_1, x_2, -L_3) = -\mathbf{q}(x_1, x_2, L_3). \end{aligned} \tag{17}$$

The formulation presented here can be used to handle particles of arbitrary shapes in arbitrary configurations. Alternatively, Zick and Homsy[34] developed a special fundamental solution that explicitly accounts for the periodicity. This special solution is less general since it depends on the configuration of the unit cell. Also, this special solution involves a summation over all particles in the particle lattice and therefore does not accommodate the splitting of the original domain for computational efficiency.

Handling of traction discontinuities at edges and corners

The second-order method employs quadratic elements, as compared with the Tran-Cong *et al.*[4,5] approach of using constant elements. Since in a quadratic element the unknowns are placed on the edges of the element, some of the unknowns are assigned at the edges of the unit cell (see Figure 3). This poses a special challenge in numerical implementation, since two (or three) unknowns can exist at the same node on the edge (or at the corner) of the unit cell. When the unknowns are all velocities, these unknowns are required to have the same value owing to the continuity of the variable in the quadratic element. Thus the number of unknowns is reduced. On the other hand, when some of the unknowns at the same node are tractions, the situation becomes more difficult. Recall that traction $\mathbf{q} = \sigma \cdot \mathbf{n}$. The unknowns at the same node correspond to different directions of $\mathbf{n}$ and the unknowns in general are not equal. Hence there are more unknowns than equations rendering the G-matrix singular. This problem of multiple unknowns at the same node also exist when using the BEM to solve 2D physical problems, in which case at the corners of the domain there are two unknowns per corner node.

The handling of traction discontinuities at the edges/corners is critical for the numerical solution, hence the treatment of the periodic boundary conditions requires special care. Yan and Lin[35] discussed some of the solutions to treat the corners.

1. Assume that the traction is continuous at corners, so only one unknown traction needs to be determined.
2. Allow a gap between the elements around the corner (Figure 4(a). Thus the boundary of the flow domain is discontinuous. The gap is usually small, so reasonable accuracy is obtained.
3. Split the corner into two nodes, with each moved a small distance away from the corner (Figure 4(b). The value at the corner is then extrapolated from the nodal values.
4. Use constant elements near edges/corners (Figure 4(c) and higher-order elements everywhere else. Link elements are needed to connect constant elements to higher-order elements.
5. Use a so-called boundary point element which is essentially a modified linear element with two nodes but zero length. With the two nodes the two tractions can be determined.
6. Gray[36] used additional collocation nodes to generate the extra equations. They can be placed outside the fluid domain, so the LHS of the integral equation (3) is zero. The exact locations of the extra nodes are critical and can only be found from numerical experiments.

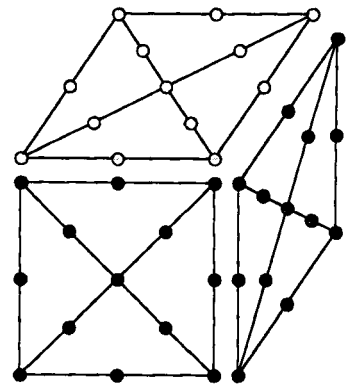

Figure 3. Existence of multiple unknowns at the edges and corners of the unit cell. Here the surfaces of the unit cell are slightly displaced to show the location of the unknowns

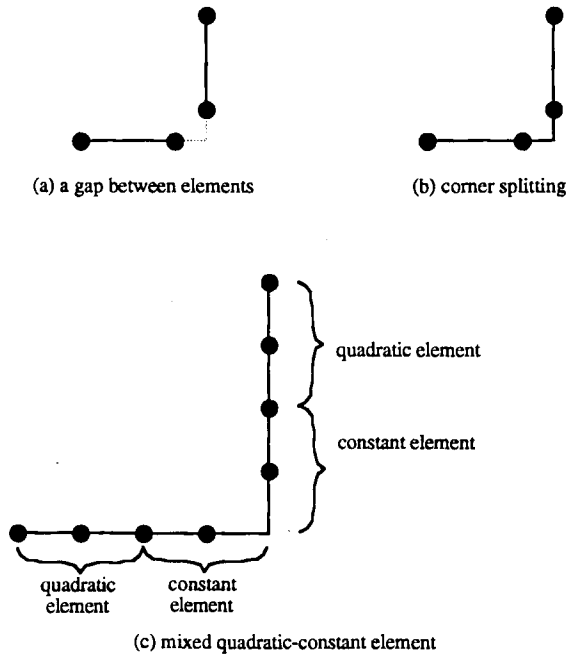

Figure 4. Treatment of corners: (a) a gap between elements—the dotted line shows the actual boundary of the domain; (b) corner splitting; (c) mixed order of elements

The above discussion pertains to applications in 2D physical problems. By comparison, less work has been done on 3D physical problems, but similar schemes are usually recommended. The cases of a simple shear and a Poiseuille flow field were used to test the usefulness of these approaches. The condition numbers and errors for the approaches tried are given in Table I. The first approach was not tried in this study since it is clearly unacceptable. The second approach was also not tried since the solution accuracy depends significantly on the gap size, which cannot be optimized *a priori*.

For approach #3 there are two possible ways of implementation. First, the edge/corner nodes can be moved along the edge as shown in Figure 5. The **G**-matrix was found to be singular irrespective of how the nodes are moved. A check revealed that the two sides of the discretized integral equation (10) did not match. Further investigation showed that the unknowns go

Table I. Condition numbers and errors in the various approaches tried to handle edges/corners

Approach	Description	Condition number	Error*
#3a	Move nodes along edges	10^{18}	10^{11}
#3b	Move nodes inwards towards inside	10^{7}	10^{-4}
#6	Use additional collocation nodes	10^{10}–10^{18}	10^{2}–10^{10}
#7	Galerkin BEM	10^{7}	10^{-4}

* Errors were measured by the L_2-norm.

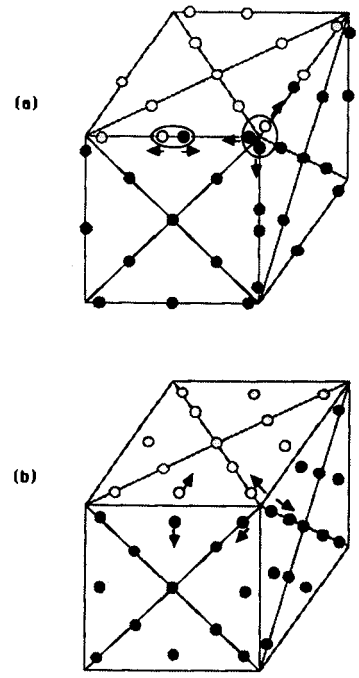

Figure 5. The two implementations of approach #3 in the treatment of corners: (a) nodes are moved along the edges; (b) nodes are moved inwards towards the interior

through a jump in values when one moves the node from one surface to the next. This jump can be determined analytically and the procedures are given in Reference 37. After this adjustment the two sides of the integral equations were shown to agree within 10^{-6} in the two test cases of shear and Poiseuille flow. However, even then the condition number of the resulting matrix **G** was still very high. In fact, the existence of such a high condition number should not be surprising; locally there are more equations than unknowns.

In the second implementation of approach #3 the nodes from the edges/corners are moved inwards towards the inside of the element. This approach is very similar to the quarter-point technique in finite element technology used for handling local singular variables. In the FEM it has been demonstrated in quadrilateral elements that placing the node one-quarter away from the singularity point yields the best results (see e.g. Reference 38). This scheme was tried on the simple mesh shown in Figure 5 and was shown to provide very good accuracy—the tractions in the shear flow test case were determined within 0·01%. Indeed, the solution did not appear to be highly sensitive to how far inside the element the nodes are moved. Moving them from $\eta = 0{\cdot}8$ to $\eta = 0{\cdot}95$ yielded similar results, where the local variable $\eta = 1$ denotes the corner. The condition number of the matrix became very high and the solution accuracy degraded only when the nodes were moved closer to the corner. However, such an approach is cumbersome for mesh refinement studies when triangular elements are used, especially when some of the triangular elements have the sides at an angle to the edge. The nodes can be moved inwards by arbitrarily assigning them to one of the two adjacent elements. However, this arbitrariness renders a uniform mesh refinement meaningless.

Approaches #4 and #5 were not tried since they reduce the local accuracy significantly, thus undermining the overall idea of using quadratic elements.

Although it was shown by Gray[36] to work in the 2D case, approach #6 yielded a matrix with very high condition number in our 3D test cases irrespective of how far the extra collocation nodes were placed outside the domain. Although this approach is appealing from the theoretical point of view, its implementation appears to be difficult owing to the high sensitivity to the placement of the nodes.

Of the many approaches discussed so far, the discontinuous element approach #3b performed the best. However, it does not permit uniform mesh refinement, which is a key to determining numerical convergence. Note that the above discussion has pertained to using the boundary collocation method in which the integral equation is required to be satisfied at the collocation node. It is well known in both the FEM and BEM that in such a method the accuracy of the numerical solution depends greatly on the location of the collocation nodes. The experience with approaches #3 and #6 has surely supported this. It is therefore clear that if the errors at the collocation nodes are averaged, sensitivity to the nodal location will be reduced. This averaging scheme, for example, can be implemented by weighting the integral equation by a weighting function. Therefore a Galerkin formulation appears to be well suited for the application and was tried as approach #7.

Galerkin boundary element method

In the Galerkin formulation the integral equation (3) is weighted by the interpolation function ϕ_g:

$$\int_{\Gamma_y} \phi_g c(\mathbf{y}) u_i(\mathbf{y})\, d\Gamma_y = \int_{\Gamma_y}\int_{\Gamma_\zeta} \phi_g u^*_{ij}(\mathbf{y}, \zeta) q_j(\zeta)\, d\Gamma_y\, d\Gamma_\zeta + \int_{\Gamma_y}\int_{\Gamma_\zeta} \phi_g \sigma^*_{ijk}(\mathbf{y}, \zeta) n_k(\zeta) u_j(\zeta)\, d\Gamma_y\, d\Gamma_\zeta. \quad (18)$$

It is important to point out the difference between the collocation and Galerkin formulations. The difference is that in the collocation formulation the integral equation is expressed with reference to the nodes at which the unknown variable (**u** or **q**) is sought. In the Galerkin formulation the integration of the integral equation is numerically evaluated at exterior collocation nodes which do not have to coincide with the variable nodes. The collocation nodes are usually the locations of Gauss points. Figure 6 shows examples of the collocation nodes in both formulations. At first glance it may appear that the Galerkin formulation requires much more computational effort. As shown in the one-element example problem, only six collocation nodes are used in the collocation nodes and the integral equation is evaluated six times. In

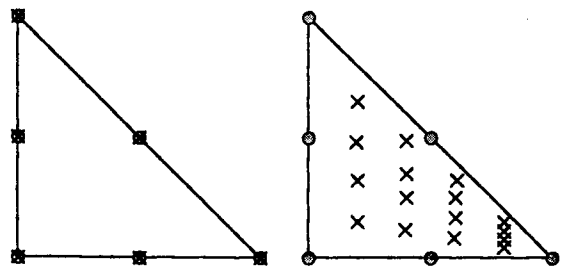

Figure 6. Location of the collocation nodes (marked by crosses); variable nodes are marked by circles: (a) collocation formulation; (b) Galerkin formulation

comparison, 16 collocation nodes are used in the Galerkin formulation. For each variable node the integral equation has to be evaluated 16 times. Altogether, 96 evaluations are required! However, in practice, at each collocation node the contribution of the integral equation to each of the six variable nodes is determined. Thus only 16 evaluations of the integral equation are needed. Therefore this example shows that although the Galerkin formulation requires more computation than the collocation formulation, the computational formulation, the computational load increase is not too large, typically about threefold.

NUMERICAL IMPLEMENTATION

The numerical implementation of the Galerkin BEM technique in the collocation formulation is straightforward. In the existing algorithm for the collocation formulation only the weighting by the weighting function needs to be implemented to switch over to the Galerkin formulation. However, an additional modification is required. The adaptive subdomain integration scheme introduced in our previous paper[20] was found to successfully remove the near singularities in the non-singular integrations. In essence, the integration domain was subdivided into subdomains, with the length of the subdomain being halved during each subdivision (see Figure 7). The process of subdivision was continued until the sum of the integrals in the subdomains agreed with the integral evaluated in the parent domain within a convergence criterion (typically 10^{-8} of the normalized sum of the components in a row).

In the collocation BEM scheme all the collocation nodes were on the edges or at the corners

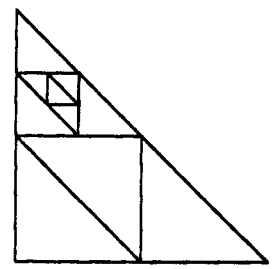

for isoparametric element

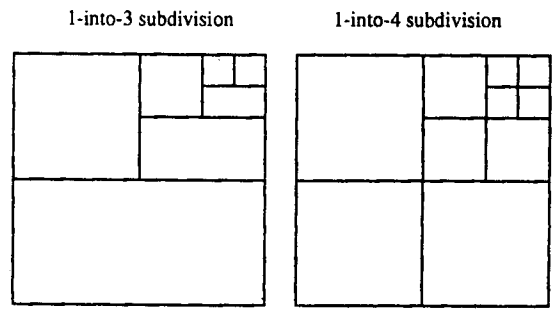

for superparametric element

Figure 7. Subdomain integration scheme

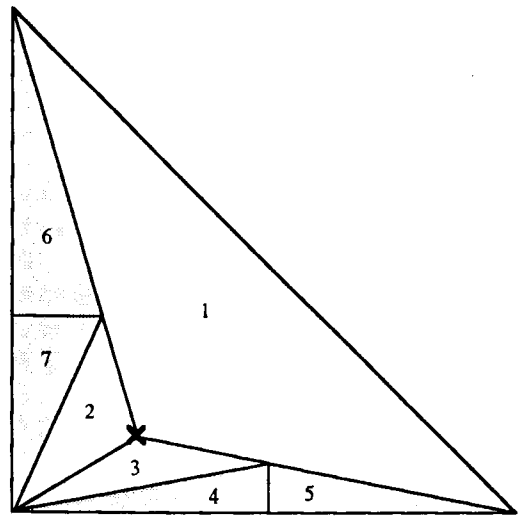

Figure 8. Subdivision used in singular integration, with the cross denoting the collocation node. Singular integration is performed in subdomains 1–3 and non-singular integration is performed in subdomains 4–7

of the element. The singular integration by polar co-ordinate transformation was found to perform very well. In the Galerkin BEM technique the collocation nodes are distributed inside the element. At some locations the collocation nodes are very close to the edge or the corner. Clearly, the singular integration scheme developed was not sufficient to handle the internal collocation node and needed to be modified.

First, the scheme of subdividing the domain into three singular integration subdomains was tried but was found to yield errors of the order of 1%, expecially in cases where the collocaiton nodes are close to the edge of the element. A subsequent numerical investigation showed that in such cases some of the subdomains are very elongated. It was found that as a rule an element aspect ratio of greater than eight will introduce errors in the calculation of the area of over 2%. For such large element aspect ratios increasing the number of Gauss points in the singular integration did not improve the accuracy significantly, since the Gauss points are mostly populated towards the centre of the subdomain.

A modified singular integration scheme was used as depicted in Figure 8. With this scheme it is possible to control the accuracy in the integration of any arbitrary function. It is in principle similar to the non-singular subdivision scheme. In essence, the integration domain is subdivided into two groups of subdomains. In the first group singular integration is performed within the subdomain. In the second group non-singular integration is performed within the subdomain. The error in the non-singular integration scheme is monitored and further subdivisions are carried out until convergence is achieved. On the other hand, the convergence in the singular integration scheme is achieved by increasing the number of Gauss points.

RESULTS AND DISCUSSION

Case 1. Convergence studies in smooth problems

The example problem of flow past two rigid spheres in an unbounded domain was first considered in order to study the convergence of the Galerkin BEM technique. Results were

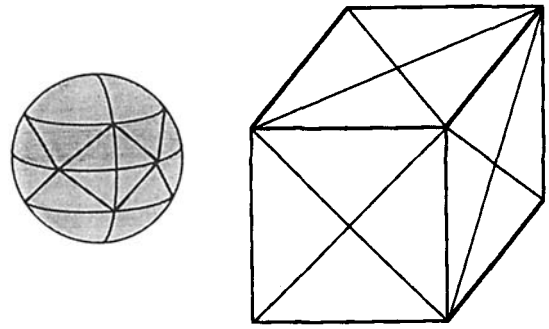

Figure 9. Mesh used for studying spherical suspensions (24-element for the unit cell and 32-element for the sphere)

compared with the analytic solutions.[33] In discretizing the surface, triangular elements were used which allowed easy local mesh refinement at points where large gradients of stresses were anticipated. A typical mesh is shown in Figure 9.

For flow past a sphere in an unbounded domain the Stokes law is applicable and the drag force is given by $F_D = 6\pi\mu U a_s$, where U is the far-field velocity and a_s is the sphere radius. For flow past a particle of arbitrary shape or past many particles the Stokes law is modified to give $F_D = 6\pi\mu U a_e R$, where a_e is the radius of the sphere with the same volume as the particle and R is a dimensionless drag ratio describing the effect of particle shape and particle–particle interactions. Similarly the dimensionless rotational velocity is defined as $\omega^* = \omega a_s/U$.

The convergence of the technique was studied using mesh refinement. We studied the case of flow past two nearly touching spheres, which is considered to be a numerically difficult task.[4,20] As seen in Table II, the error in the drag ratio (and thus the translational velocity) decreased from 3% using the coarse mesh to less than 0·4% using the fine mesh. The fact that we even obtained convergence is attributed to the use of the subdivision integration schemes. As seen, the relative error in the calculation of the rotational velocity was higher than that of the translational velocity, but nonetheless convergence was achieved at all gap sizes.

Mesh refinement was used to improve the numerical efficiency. Since high stresses exist in the interparticle or particle–wall gap, elements in the gap region were locally refined. Based on the uniformly spaced 32-element mesh, locally refined meshes of 48 and 64 elements were generated. As shown in our previous paper,[20] using the 48-element locally refined mesh yielded the same accuracy as the 128-element uniform mesh but required only a fraction of the CPU time.

Case 2. Suspension of spheres

For a dilute suspension of spheres Einstein[39] proved that the viscosity depends linearly on the sphere concentration:

$$\mu_{rel} = \mu_{eff/\mu fluid} = 1 + 2{\cdot}5\, V_s, \tag{19}$$

where μ_{rel} is the relative viscosity, also called the reduced viscosity, defined as the ratio of the effective viscosity of the suspension to the viscosity of the suspending fluid, and V_s is the concentration of spheres in the suspension expressed as a volume fraction. Since this relationship was derived for a dilute suspension, various high-order corrections to it have been proposed. Several corrections can be found in the classic book by Happel and Brenner.[33]

To verify the second-order Galerkin BEM, the problem of a suspension of spheres in shear

Table II. Flow past two nearly touching spheres using the Galerkin BEM with isoparametric elements

Gap/dia	Elements	Condition number	Drag ratio	Error	Rotational velocity	Error
0·01000	8	$1{\cdot}61 \times 10^5$	0·68470	−0·02794	0·10939	0·02146
	32	$5{\cdot}84 \times 10^5$	0·70877	−0·00387	0·09754	0·00961
	48	$8{\cdot}11 \times 10^6$	0·71033	−0·00231	0·08959	0·00166
	64	$1{\cdot}09 \times 10^7$	0·71068	−0·00196	0·08732	−0·00061
	Exact		0·71264		0·08793	
0·00245	8	1.61×10^5	0·68324	−0·02967	0·10997	0·03280
	32	5.84×10^6	0·70749	−0·00542	0·09654	0·01937
	48	8.60×10^6	0·70952	−0·00339	0·08561	0·00844
	64	$2{\cdot}54 \times 10^8$	0·71059	−0·00232	0·07863	0·00146
	Exact		0·71291		0·07717	
0·00050	8	1.61×10^5	0·68286	−0·03128	0·11011	0·04303
	32	5.84×10^6	0·70717	−0·00697	0·09624	0·02916
	48	8.68×10^6	0·70934	−0·00480	0·08440	0·01732
	64	$4{\cdot}13 \times 10^8$	0·71079	−0·00335	0·07498	0·00790
	Exact		0·71414		0·06708	
0·00010	8	1.61×10^5	0·68278	−0·03255	0·11014	0·05106
	32	5.84×10^6	0·70710	−0·00823	0·09618	0·03710
	48	$8{\cdot}69 \times 10^6$	0·70930	−0·00603	0·08414	0·02506
	64	$3{\cdot}65 \times 10^8$	0·71085	−0·00448	0·07413	0·01505
	Exact		0·71533		0·05908	

flow was studied. Length was scaled by the larger dimension of the particle and time was scaled by the inverse of the imposed strain rate. A single sphere was used which was placed in the centre of the cell. Figure 9 shows the typical 24-element mesh used for the unit cell. For convenience a cubic unit cell was used in this study, but the BEM offers the flexibility of choosing any geometry for the unit cell. To change the concentration of the suspension, we chose to vary the size of the sphere relative to a fixed size unit cell. The motion of the sphere was calcualted directly from solving the mobility matrix **G**. The resulting viscosity of the suspension was calculated using Batchelor's formalism.

Owing to the homogeneity of shear flow, there is no translational velocity. As seen in Table III, an eight-element mesh was initially used for the sphere and was found to give an 11% error on the viscosity coefficient in equation (19). The large error was traced to the fact that the sphere volume was approximated with a 15% error using the eight-element mesh. Upon correcting for the volume, the error in the viscosity coefficient was reduced to about 3·9%. The error on the rotational velocity is so small that a reliable convergence order could not be determined. Based on the viscosity coefficient from the first two meshes, the convergence order was determined to be 2·9. (Note that the error using the fine mesh was so small that the numerical error was masked by the computer truncation error.) Therefore the actual convergence order was above 2·9. The 32-element mesh was selected for use in the rest of this study as the best compromise between accuracy and CPU requirements.

Two ways of implementing the periodic conditions were tested in this study. In the first case the periodic boundary conditions were the same as those used by Tran-Cong *et al.*[5,22] In essence, the shear flow studied here is a periodic flow in two directions bounded by two solid parallel

Table III. Uniform mesh refinement results on the motion and viscosity of a suspension of spheres in shear flow in the x_1-direction. The sphere volume fraction was 0·01. Periodicity was prescribed in the x_2- and x_3-directions only

Elements used	ω_2	Viscosity coefficient before volume adjustment	Viscosity coefficient after volume adjustment
8 on sphere, 12 on unit cell	0·4995	2·211	2·598
32 on sphere, 48 on unit cell	0·5001	2·476	2·513
128 on sphere, 192 on unit cell	0·5000	2·497	2·500

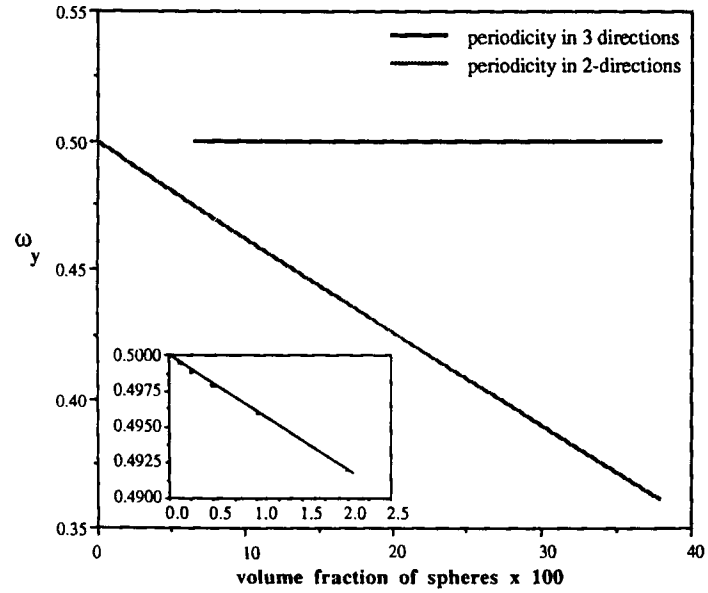

Figure 10. Rotational velocity of a sphere in the unit cell of a suspension

plates. As shown by the 'jagged' curve in Figure 10, the rotational velocity decreases as the concentration increases, indicating that the motion is suppressed by the sphere–wall interaction. In the very dilute limite where Einstein's approximation holds, the rotational velocity approaches asymptotically a value of 0·5000 ± 0·0001, compared with the exact value of 0·5. In comparison, the asymptotic value obtained by Tran-Cong *et al.*[5] using constant elements was 0·502.

From the particle extra stress the 'instantaneous effective' suspension viscosity can be determined. It can be seen from Figure 11 that in the dilute limit the slope of the viscosity–concentration curve is 2·500 ± 0·001, compared with the exact value of 2·500. The dependence of the shear component of the particle extra stress was similar to that observed by Tran–Cong *et al.*[5] Also as reported by them, there was no normal stress difference over the whole concentration range. Indeed, the individual normal components in the particle extra stress tensor were negligible. Note that at high concentrations the simulation result is probably not realistic owing to the use of a highly structured unit cell (containing only a single sphere) to approximate a concentrated suspension in which the interparticle spacing is irregular.

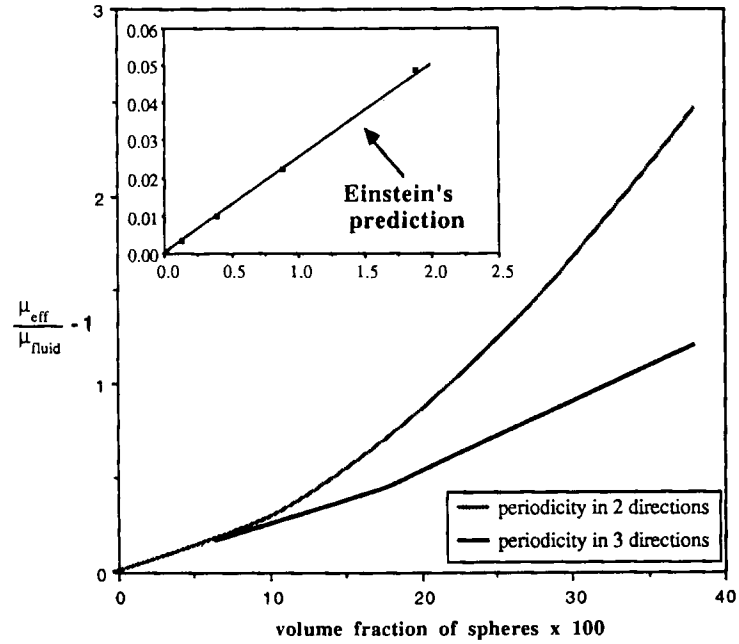

Figure 11. Effective viscosity of the sphere suspension

In the second case the periodic boundary conditions were applied in all three directions. The sphere was shown to be rotating at a velocity of only slightly below 0·5 for the whole range of concentration studied. At the highest concentration studied, $V_s = 0{\cdot}38$, the rotational velocity is about 0·4994. This is consistent with the result of Nunan and Keller,[40] who showed that the angular velocity of the sphere should be exactly half of the curl of the average velocity, independently of the volume fraction. As noted by Nunan and Keller, this is the same angular velocity that the sphere will experience in an unbounded domain of shear flow with the same shear strain. In other words, in each unit cell the sphere is spinning as if it is alone.

In this case the shear particle extra stress actually followed Einstein's predicted value quite closely over a larger range of concentrations. In other words, owing to the absence of the wall effect, the extra stress is smaller in this case. Also, significant normal stress, at the level of as much as 30% in magnitude of the shear stress in the case of $V_s = 0{\cdot}38$, was observed. However, both the first and second normal stress differences were zero. (The normal stress arises from squeezing the fluid in the gap between the two spheres.) As explained by Brady and Bossis,[41] normal stress differences results from an angular anisotropy in the sphere configuration, which was absent in this study.

Two conclusions can be drawn from this excursion into the rheology of spherical suspensions. First, the numerical solution for the unit cell is sensitive to the implementation of the periodic boundary conditions. Usually periodicity in all three directions is desired. In order to achieve this, Tran-Cong *et al.*[5,22] had to resort to using multiple (two, three or four) layers of spheres between the solid plates. Even then the result using four layers was still 2% different from that using three layers, thus indicating that some effect of the wall was still present. The implementation used in this study represents a significant improvement over the approach taken by Tran-Cong *et al.* and was used for the rest of the study. Secondly, the wall effect is shown to be very significant.

Case 3. Flow of ellipsoidal particle suspensions

Jeffery[42] studied the particle motion and rheology in a suspension of ellipsoidal particles. To describe the angular velocities, the spherical co-ordinate system with solid angles ϕ and θ is used (see Figure 12). For shear flow the rates of change of these angles ($\dot{\phi}$ and $\dot{\theta}$) with respect to time, which completely describes the three-dimensional particle rotation, are

$$\dot{\phi} = \frac{\dot{\gamma}}{r_p^2 + 1}(r_p^2 \cos^2 \phi + \sin^2 \phi), \tag{20}$$

$$\dot{\theta} = \frac{\dot{\gamma}(r_p^2 - 1)}{4(r_p^2 + 1)} \sin(2\phi)\sin(2\theta), \tag{21}$$

where r_p is the ellipsoid aspect ratio and $\dot{\gamma}$ is the shear rate.

For an ellipsoid, according to equation (20), the motion is periodic. $\dot{\phi}$ has maxima at $\phi = 0$ and π. The corresponding minima of $\dot{\phi}$, which are not zero, occur at $\phi = \pi/2$ and $3\pi/2$. Thus the ellipsoid spends most of its time in an orientation close to the flow direction. At every half-period it experiences a rapid change in the orientation by tumbling 180°. Integration of equation (20) shows that the rotation of the spheroid is periodic, with the angle ϕ depending on only r_p and the shear strain $\dot{\gamma}t$:

$$\tan \phi = r_p \tan\left(\frac{\dot{\gamma}t}{r_p + 1/r_p}\right), \tag{22}$$

with a period of rotation

$$T_{rot} = \frac{2\pi}{\dot{\gamma}}\left(r_p + \frac{1}{r_p}\right). \tag{23}$$

In a suspension where there are many fibres, a description of the orientation states of individual particles is impractical. Advani and Tucker[43] showed that the most concise and compact way to describe the orientation distribution is through the moments of the distribution function, e.g. the second-order orientation tensor

$$a_{ij} = \int \mathbf{p}_i \mathbf{p}_j \psi(\mathbf{p})\, d\mathbf{p} \tag{24}$$

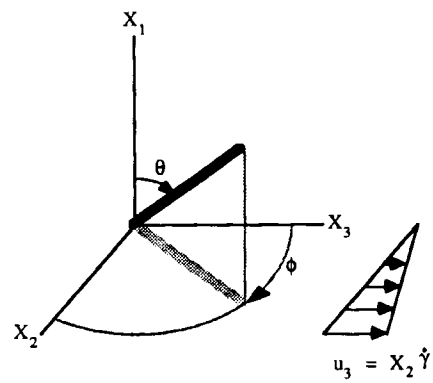

Figure 12. Fibre orientation in the fixed co-ordinate system (X_1, X_2, X_3), where X_1 is the polar axis and $\phi = 0$ when the fibre is oriented at the flow direction

and the fourth-order orientation tensor

$$a_{ijkl} = \int \mathbf{p}_i\mathbf{p}_j\mathbf{p}_k\mathbf{p}_l\psi(\mathbf{p})\,d\mathbf{p}, \tag{25}$$

where $\mathbf{p}$ is a unit vector related to θ and ϕ that describes the orientation and $\psi(\mathbf{p})$ or $\psi(\theta, \phi, t)$ is the distribution function, which is defined as the probability density of finding a particle oriented within a small solid angle $\sin\theta\,d\theta\,d\phi$ around the direction (θ, ϕ) at time t.

Based on the earlier work by Hinch and Leal,[44] Tucker[45] developed an expression for the particle extra stress in an arbitrary flow as a function of the ellipsoid orientation distribution and concentration:

$$\sigma_{ij}^{(p)} = \mu V_f[A\dot{\gamma}_{kl}a_{ijkl} + B(\dot{\gamma}_{ik}a_{kj} + \dot{\gamma}_{jk}a_{ki}) + C\dot{\gamma}_{ij}], \tag{26}$$

where A, B and C are shape coefficients that depend only on the particle aspect ratio and concentation and not on the orientation state of the particles.

In this study three values of aspect ratio were studied: 18, 36 and 54. For convergence studies only the ellipsoid with $r_p = 18$ in a dilute suspension was considered. In general, more elements are needed to approximate a spheroid than a sphere. Typically either a 24-element or a 40-element mesh was used. The size of the particle can be set arbitrarily as long as the interparticle spacing is consistent with the requirement that the fibre should rotate freely inside the box. Using too short a particle will make it very small relative to the unit cell. Using too long a particle will violate the assumption of a dilute suspension. Based on these considerations, a ratio of fibre length to the length of the box of 0·45 was used originally. At that length a fibre of aspect ratio 18 occupies only about 0·03% of the unit cell volume. As an numerical experiment the fibre length was extended to twice the original volume while maintaining the same aspect ratio of 18. In other words, the ratio of fibre length to unit-cell length was increased from 0·45 to 0·90. As seen in Table IV, the resulting coefficients are essentially the same.

First the effect of mesh size and ratio f fibre length to unit-cell length was investigated. Figure 13 shows the rotational velocity of the bifre when it is oriented in the shear plane, i.e. $\theta = \pi/2$. In this case only $\dot{\phi}$ is non-zero. The velocity is presented on a logarithmic scale to show that the maximum and minimum rotational velocities differ by a ratio of r_p^2. As can be seen, the predicted motion using the 24-element and 40-element meshes is indistinguishable from the

Table IV. Coefficients in the particle extra stress equation determined from multiple regression

Case	Formulation	Aspect ratio	Elements on ellipsoid	L_f/L_{box}	Equation used	A	B	C
I	Galerkin	18	24	0·45	$\sigma_{12}^{(p)}$	73·64	0·03	2·024
II	Galerkin	18	40	0·45	$\sigma_{12}^{(p)}$	73·86	0·04	2·003
III	Galerkin	18	40	0·90	$\sigma_{12}^{(p)}$	75·42	0·06	2·003
IV	Galerkin–collocation	18	24	0·45	$\sigma_{12}^{(p)}$	73·76	0·04	2·088
V	Galerkin–collocation	18	40	0·90	$\sigma_{12}^{(p)}$	76·07	0·08	2·001
VI	Galerkin–collocation	36	40	0·90	$\sigma_{12}^{(p)}$	234·3	0·2	2·000
VII	Galerkin–collocation	54	40	0·90	$\sigma_{12}^{(p)}$	463·4	0·4	2·000
	Exact	18				73·82	0·017	2·037
		36				229·7	0·006	2·012
		54				454·6	0·003	2·006

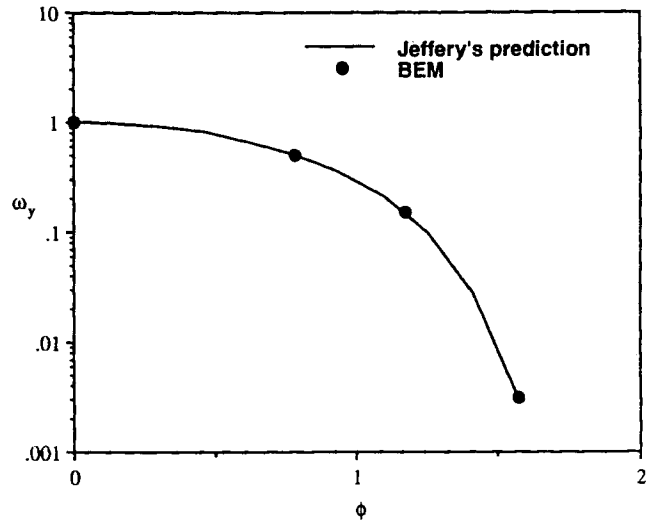

Figure 13. Rotational velocity of an ellipsoid under simple shear flow of a unit strain rate. The BEM results were obtained using the Galerkin formulation with a 40-element mesh on the ellipsoid and a 24-element mesh on the unit cell

analytic results. In fact, the performance of the Galerkin BEM technique surpassed the original expectation of the study by providing high accuracy even from such coarse meshes.

From the particle extra stress the coefficients can be determined. As shown in Figure 14, coefficient A is the dominant one and is about three to four orders of magnitude higher than coefficient B. Indeed, as the aspect ratio increases, A increases and B decreases. At the higher values of aspect ratio B is so small that the influence of B on the stresses can be safely neglected. On the other hand, coefficient C remains nearly constant over the whole range of aspect ratios

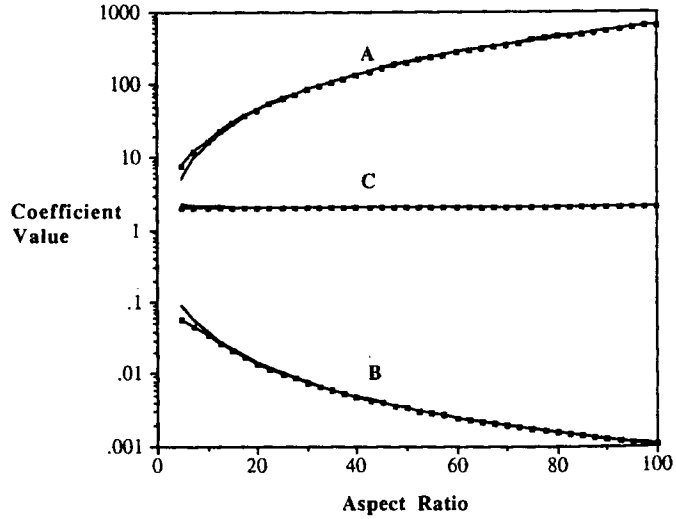

Figure 14. Analytic (———) and asymptotic (—□—) values of the coefficients in the particle extra stress equation

and has a value of just slightly over two. Note that the asymptotic values obtained by Hinch and Leal[44] using the slender body approximation are within 15% of the exact values at $r_p = 10$ and within 1% when $r_p = 50$. In this study the three unknowns A, B and C were determined by multiple regression of the data at five different ellipsoid orientations. Note that for particles that lie in the shear plane, there are only three non zero stress components, $\sigma_{12}^{(p)}$, $\sigma_{11}^{(p)}$ and $\sigma_{22}^{(p)}$, and that coefficient C appears only in the in-plane shear stress:

$$\begin{aligned} \sigma_{11}^{(p)} &= \mu V_f \dot{\gamma}_{12}(2Aa_{1112} + 2Ba_{12}), \\ \sigma_{12}^{(p)} &= \mu V_f \dot{\gamma}_{12}[2Aa_{1122} + B(a_{11} + a_{22}) + C], \\ \sigma_{22}^{(p)} &= \mu V_f \dot{\gamma}_{12}(2Aa_{1222} + 2Ba_{12}). \end{aligned} \tag{27}$$

As seen in Table IV, the agreement with the BEM solution is excellent, with typical errors of about 2%. Figure 15 shows the profile of the three non-zero components of the particle extra stress.

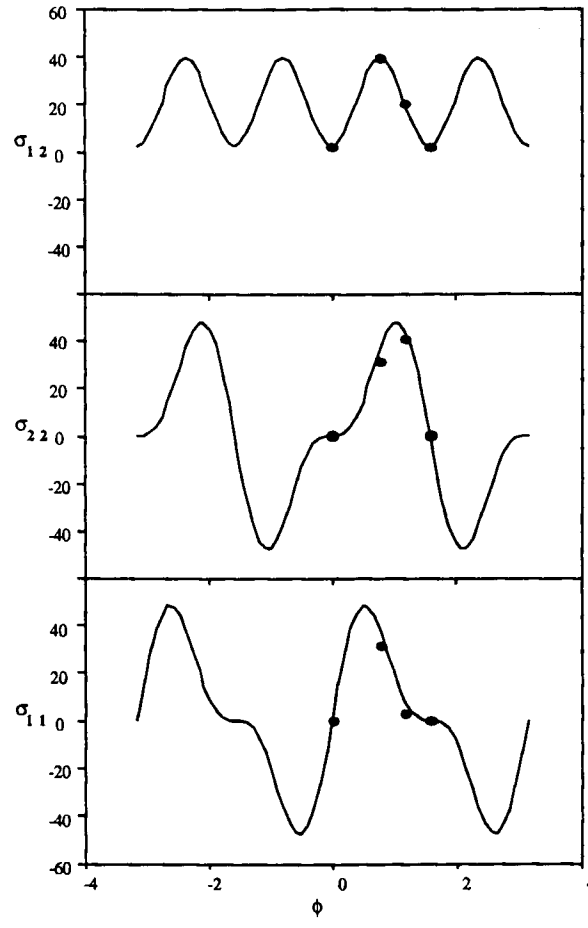

Figure 15. Particle extra stress as a function of the in-plane angle: ●, BEM solution using the Galerkin formulation with 40 elements on the ellipsoid; ———, Jeffery's prediction

So far, the results discussed have focused on having a single particle in the unit cell. To check if the unit-cell approach and the periodic boundary conditions had been implemented correctly, two unit cells were fused together and a fibre placed in each half-cell with identical orientation ($\theta = \pi/2$, $\phi = \pi/2$). The choice of $\phi = \pi/2$ was based on the observation that accuracy at small rotational velocities was more difficult to achieve than at high rotational velocities. The rotational velocities of the two fibres were within 0·15%, indicating that the implementation of periodicity was correct.[37] In this case the ratio of fibre length to unit-cell length was 0·45. The rotational velocity from each fibre in the fused box was 3·6% higher than that from the single fibre in a box, thus indicating a slight interaction even at such a dilute suspension. On the other hand, the particle extra stress from each fibre in the fused box was only 0·02% higher than that from the single fibre in a box.

Finally, it is worth mentioning that the condition number for the many cases discussed so far was of the order of 10^9–10^{10}. Despite such high numbers, the solution was stable in all cases.

Case 4. Galerkin–collocation method

From the above analyses it can be seen that the Galerkin formulation gives very accurate results but the CPU requirement is high. One way to reduce the CPU requirement is to evaluate the integral equations on the particle using the collocation formulation. Recall that the use of the Galerkin formulation was motivated by the need to handle corners. Since the particle does not have corners, the Galerkin formulation is not needed. The collocation formulation, which requires one-third to one-quarter the CPU required by the Galerkin formulation, is thus attractive for evaluating the integral equations at collocation nodes on the particle.

To check the validity of the scheme, the same five orientations of the ellipsoid of aspect ratio 18 were evaluated using the mixed Galerkin–collocation formulation. The results are given in Table IV. The errors were higher in this case as expected, but not by much. The error in the coefficients was about 3·7% in the 24-element mesh and 2·8% in the 40-element mesh. Thus this scheme offers a significant saving in the CPU requirement while maintaining a reasonable level of accuracy. Since the Galerkin–collocation formulation results were not too far from the Galerkin formulation, the CPU consideration favours the use of the former formulation.

Case 5. Effect of cylindrical shape of fibres on suspension properties

In reality the fibres are cylindrical instead of ellipsoidal in shape. Hence it is of interest to understand how Jeffery's equations can be extended to a more general particle shape. One noticeable difference between cylinders and ellipsoids is that cylinders have blunt ends whereas ellipsoids have round ends. Intuitively one would expect that if the fluid is flowing in the fibre direction, the blunt end will provide excess drag. Also, during rotation a cylinder will have a larger moment than an ellipsoid of the same major and minor semi-axes owing to the larger cross-section at the ends.

In their experimental study of rods Goldsmith and Mason[46] defined an equivalent ellipsoidal axis rato r_e for cylindrical particles with actual axis ratio r_p, based on the period of rotation of the cylinders. They found that the ratio of r_e/r_p decreased from 0·72 to 0·57 as r_p increased from 18 to 130. In his study on the slender body approximation Burgers[47] found theoretically that r_e/r_p was about 0·74. Thus equation (20) can be used to describe the motion of a cylinder in shear flow by substituting r_e for r_p. Little work has been done to determine if the rheological model for ellipsoids, equation (26), can be modified for cylinders through the use of the same concept of r_e.

Equation (20) shows that the rotational velocity is a function of both the aspect ratio (in this case r_e is used instead of r_p) and the orientation. Specifically, the second term in this equation, prevalent for ϕ around $\pi/2$, is proportional to $1/(r_e^2 + 1)$ and is thus very sensitive to the value of r_e. Hence a single value at $\phi = \pi/2$ is sufficient to determine r_e, since the first term is zero. Physically speaking, since the period of rotation is controlled by the small rotational velocities around $\phi = \pi/2$, this simple determination of r_e is logical.

As shown in Figure 16, the equivalent ellipsoidal aspect ratio was found to agree within 4% with both the experimental value by Harris and Pittman[48] and the prediction by Cox.[49] The high accuracy in determining r_e is a reflection of the high accuracy of the Galerkin formulation in capturing the small values of the velocities. As shown in Figure 17, Burgers' prediction

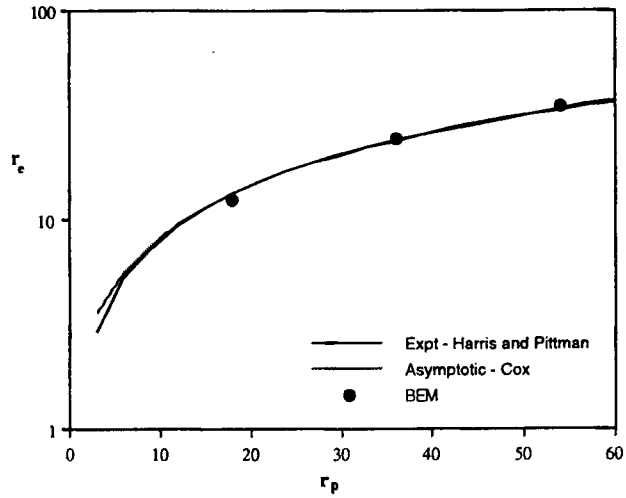

Figure 16. Equivalent ellipsoidal ratios for cylinders

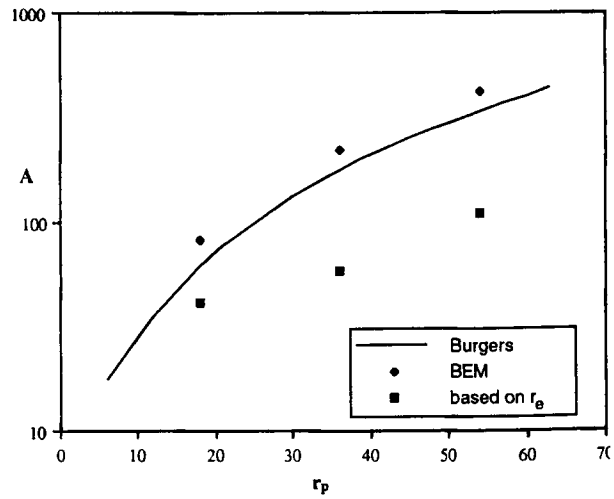

Figure 17. Values of coefficient A in a suspension of cylinders

underpredicts the extra stress by about 26% at $r_p = 18$ to 20% at $r_p = 54$. It seems that the error from Burgers' prediction drops at higher r_p-values, but this point was not exploited in the study. A comparison between the numerical value and the value of coefficient A calculated on the basis of r_e showed that the latter had an error of greater than 50%, which was increasing with r_p. Therefore this scheme should be avoided since it grossly underestimates the suspension viscosity. Based on these observations, it can be concluded that neither Burgers' prediction nor the equivalent ellipsoidal ratio concept provides a good approximation for the particle extra stress.

The rheology of a suspension of curved ellipsoids was also studied by Chan[37] but is omitted here for clarity.

Case 6. Flow through a fixed bed of fibres

The Galerkin BEM in conjunction with the unit-cell approach can also be used to study flow through a porous medium. Since the details of the pore geometry are generally unknown or too complex to account for, it is customary to describe the flow using average quantities which can be observed macroscopically. One such description is Darcy's law, which states that the flow rate is proportional to the pressure gradient ∇p multiplied by the ratio between the fibre bed permeability tensor, $\mathbf{k}$ and the viscosity:

$$\bar{\mathbf{u}} = (1/\mu)\mathbf{k} \cdot \nabla p, \tag{28}$$

where $\bar{\mathbf{u}}$ is the average fluid velocity. Darcy's law has a long history of use, especially in soil mechanics for a wide variety of porous media. Equation (28) is empirical, but its use is justified partly owing to its agreement with experimental measurements.

The prediction of $\mathbf{k}$ in such configurations is beyond the capabilities of the current theoretical models. Hence the permeability tensor is often determined experimentally. The problem of flow past a periodic network of cylinders is similar to the Stokes flow in a unit cell with cylinders in it. There are two differences between these two cases: (a) the boundary conditions are the pressure drop across the unit cell walls; (b) the fibres will run typically across the whole length of the unit cell, at least in one direction, thus making the mesh generation more complicated.

For benchmarks the cases of cross-flow and parallel flow in a square array were studied. By convention the fibre is considered to be in the x_2-direction. A typical mesh used is shown in Figure 18. From the simulation the dimensionless quantity $F_i/\bar{u}_i$ was calculated, where F is the force and $\bar{u}$ is the average fluid velocity. This quantity is in essence the flow resistance, thus the inverse of permeability. As shown in Figure 19, the calculated flow resistances for cross-flow agreed within 5% with the series expansion results of Sangani and Acrivos[50] over the fibre volume fraction range from 0·2 to 0·5. The higher error at high fibre volume fraction is expected, since the cylinder is very close to the unit-cell wall, introducing higher numerical errors. Hence for higher volume fractions a finer mesh is needed. For parallel flow it is seen that the agreement in the permeability with the series expansion results of Drummond and Tahir[51] was within 4%. Again the accuracy starts to drop towards the higher fibre volume fractions, indicating a need for mesh refinement.

For the case in which the mat is made of layers with different permeabilities, it is possible to predict the effective permeability by assuming that the permeabilities from the individual layers are additive.[52] Thus

$$\mathbf{k}_{\text{eff}} = \sum_{i=1}^{N_{\text{layer}}} \mathbf{k}_i h_i \Big/ \sum_{i=1}^{N_{\text{layer}}} h_i, \tag{29}$$

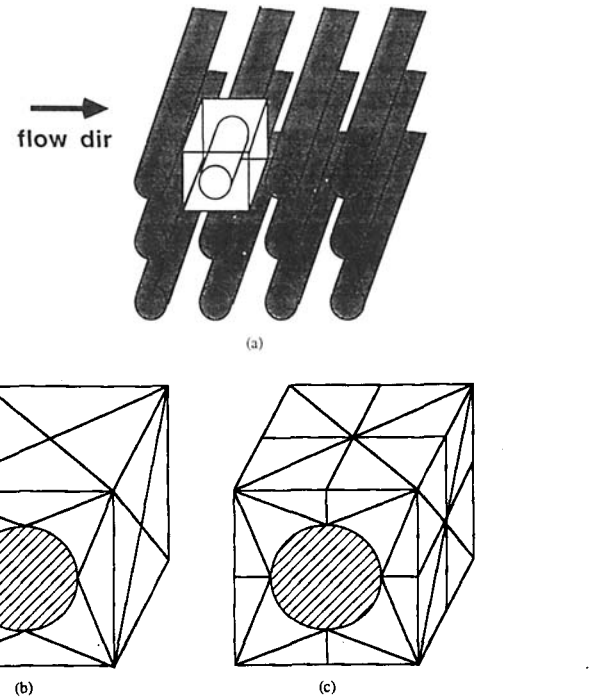

Figure 18. Mesh used in the study of cross-flow: (a) the periodic unit cell; (b) the coarser mesh; (c) the finer mesh

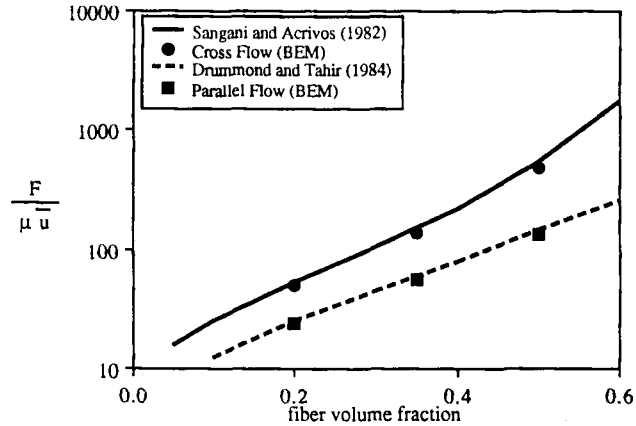

Figure 19. Flow resistance in flow past a square array of cylinders

where $\mathbf{k}_i$ and h_i are the permeability and the thickness in the ith layer respectively and N_{layer} is the total number of layers.

As shown in Figure 20, the agreement was very good at lower volume fractions but started to deviate around a fibre volume fraction of 0·35. At a fibre volume fraction of 0·50 the permeability was different by 10%. Intuitively it is reasonable that at low fibre volume fractions the cross-flow and parallel flow do not interact much but act on their respective half-cells nearly

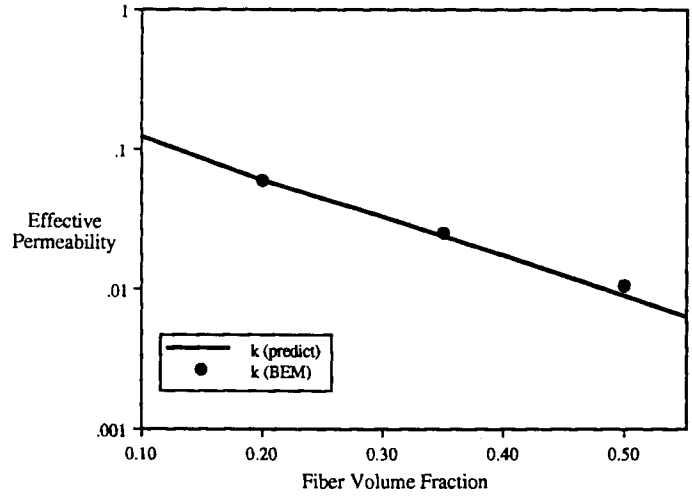

Figure 20. Permeability for the combined flow as a function of fibre volume fraction

Table V. Distribution of flow in combined parallel–cross-flow (fluid flows in the direction perpendicular to the page)

Fibre volume fraction	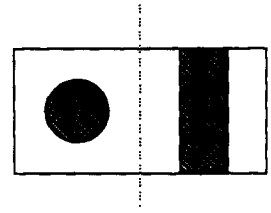	
0·20	0·56	0·44
0·35	0·57	0·43
0·50	0·61	0·39

independently. Thus equation (29) provides a good approximation. However, at high volume fractions the fluid in the low-permeability (cross-flow) half-cells starts to flow towards the high-permeability (parallel flow) half-cell. The net effect of this additional flow is to increase the permeability. This intuition is supported by examining the microhydrodynamics. From a tracer partcile study it can be clearly seen that a fraction of the fluid was moving from the low-permeability half-cell to the high-permeability half-cell. Such cell-to-cell motion was indicated by the ratio of the total flow in the high-permeability half cell. As seen in Table V, the parallel flow half-cell accounted for 56% of the total flow at a fibre volume fraction of 0·20, while this ratio increased to 61% at a fibre volume fraction of 0·50. Equation (30) does not take cross-flow into account, hence deviations from the equations at higher fibre volume fraction are expected.

ACKNOWLEDGEMENT

The authors wish to thank M. Deborah Beris for her help with the English of this paper.

REFERENCES

1. G. K. Youngren and A. Acrivos, 'Stokes flow past a particle of arbitrary shape: a numerical method of solution', *J. Fluid Mech.*, **69**, 377–403 (1975).
2. S. Kim and S. J. Karrila, *Microhydrodynamics: Principles and Selected Applications*, Butterworths, Boston, MA, 1991.
3. C. Pozrikidis, *Boundary Integral and Singularity Methods for Linearized Viscous Flow*, Cambridge University Press, Cambridge, 1992.
4. T. Tran-Cong and N. Phan-Thien, 'Stokes problems of multiparticle systems: a numerical method for arbitrary flows', *Phys. Fluids A*, **1**, 453-460 (1989).
5. T. Tran-Cong, N. Phan-Thien and A. L. Graham, 'Stokes problems of multiparticle systems: periodic arrays', *Phys. Fluids A*, **2**, 666–673 (1990).
6. S. J. Karrila and S. Kim, 'Integral equation of the second kind for Stokes flow: direct solution for physical variables and removal of inherent accuracy limitation', *Chem. Eng. Commun.*, **82**, 123–161 (1989).
7. T. Tran-Cong and N. Phan-Thien, 'Three-dimensional study of extrusion processes by Boundary Element Method. I. An implementation of high order elements and some Newtonian results', *Rehol. Acta*, **27**, 21–30 (1988).
8. P. J. Gramann, J. C. Mtzig and T. Osswald, 'Simulating the mixing of polymer blends using the Boundary Element Method', in P. Moldenaers and R. Keunings (eds.) *Theoretical and Applied Rheology, Proc. XIth Int. Congr. on Rheology*, Brussels, August 1992, Elsevier, Amsterdam, 1992, pp. 351–353.
9. P. K. Banerjee and R. Butterfield, *Boundary Element Methods in Engineering Science*, McGraw-Hill, New York, 1981.
10. C. A. Brebbia and J. Dominguez, *Boundary Elements: An Introductory Course*, 2nd edn, McGraw-Hill, New York, 1992.
11. G. Chen and J. Zhou, *Boundary Element Methods*, Academic, London, 1992.
12. G. C. Hsiao and W. I. Wendland, 'A finite element method for some integral equations of the first kind', *J. Math. Anal. Appl.*, **58**, 449–481 (1977).
13. D. N. Arnold, 'A spline-trigonometric Galerkin method and an exponentially convergent boundary integral method', *Math. Comput.*, **41**, 383–397 (1983).
14. K. E. Atkinson and A. Bogomolny, 'The discrete Galerkin method for integral equations', *Math. Comput.*, **48**, 595–616 (1987).
15. R. Rannacher and W. L. Wendland, 'On the order of pointwise convergence of some boundary element methods. Part I. Operators of negative and zero order', *Math. Modell. Numer. Anal.*, **19**, 65–88 (1985).
16. R. Rannacher and W. L. Wendland, 'Pointwise convergence of some boundary element methods. Part II', *Math. Modell. Numer. Anal.*, **22**, 343–362 (1988).
17. G. C. Hsiao, 'On the stability of integral equations of the first kind with logarithmic kernels', *Arch. Rat. Mech. Anal.*, **94**, 179–92 (1986).
18. G. C. Hsiao, 'On the stability of boundary element methods for integral equations of the first kind', in C. A. Brebbia, W. L. Wendland and G. Kuhn (eds), *Boundary Elements IX*, Vol. 1; *Mathematical and Computational Aspects*, Springer; Berlin, 1987, pp. 177–191.
19. I. H. Sloan, 'Error analysis of boundary integral methods', *Acta Numer.*, 287–339 (1991).
20. C. Y. Chan, A. N. Beris and S. G. Advani, 'Second-order boundary element method calculations of hydrodynamic interactions between particles in close proximity', *Int. j. numer. methods fluids*, **14**, 1063–1086 (1992).
21. G. K. Batchelor, 'The stress system in a suspension of force-free particles', *J. Fluid Mech.*, **41**, 545–570 (1970).
22. N. Phan-Thien, T. Tran-Cong and A. L. Graham, 'Shear flow of periodic arrays of particle clusters: a boundary element method', *J. Fluid Mech.*, **228**, 275–293 (1991).
23. G. C. Hsiao, P. Kopp and W. I. Wendland, 'A Galerkin collocation method for some integral equations of the first kind', *Computing*, **25**, 89–130 (1980).
24. G. A. Chandler and I. H. Sloan, 'Spline qualocation methods for boundary integral equations', *Numer. Math.*, **58**, 537–567 (1990).
25. K. E. Atkinson, 'The numerical solution of Laplace's equation in three dimensions II', in *Numerical Treatment of Integral Equations*, Birkhauser, Boston, MA, 1980.
26. S. Stark and A. N. Beris, 'LU decomposition optimized for a parallel computer with a hierarchical distributed memory', *Parallel Comput.*, **18**, 959–971 (1992).
27. J. J. L. Higdon, 'Stokes flow in arbitrary two-dimensional domains: shear flow over ridges and cavities', *J. Fluid Mech.*, **159**, 195–226 (1985).
28. C. Pozrikidis, 'The flow of a liquid film along a periodic wall', *J. Fluid Mech.*, **188**, 275–300 (1988).
29. M. A. Kelmanson, 'Modified integral equation solution of viscous flow near sharp corners', *Comput. Fluids*, **11**, 307–324 (1983).
30. M. A. Kelmanson, 'An integral equation method for the solution of singular slow flow problems', *J. Comput. Phys.*, **51**, 139–158 (1983).

31. O. A. Ladyzhenskaya, *The Mathematical Theory of Viscous Incompressible Flow*, Gordon and Breach, New York, 1963.
32. A. Deb and P. K. Banerjee, 'A comparison between isoparametric Lagrangian elements in 2D boundary element method', *Int. j. numer. methods eng.*, **28**, 1539–1555 (1989).
33. J. Happel and H. Brenner, *Low Reynolds Number Hydrodynamics*, Martinus Nijhoff, Dordrecht, 1983.
34. A. A. Zick and G. M. Homsy, 'Stokes flow thorugh periodic arrays of spheres', *J. Fluid Mech.*, **115**, 13–26 (1982).
35. G. Yan and F.-B. Lin, 'Treatment of corner node problems in boundary element method', in C. A. Brebbia and J. J. Connor (eds), *Proc. Eleventh Int. Conf. on Boundary Element Methods*, Springer; Berlin, 1989, pp. 215–226.
36. L. J. Gray, 'Numerical experiments with a boundary element technique for corners', in C. A. Brebbia and J. J. Connor (eds), *Proc. Eleventh Int. Conf. on Boundary Element Methods*, Springer, Berlin, 1989, pp. 243–252.
37. C. Y. Chan, 'Hydrodynamic interactions in large aspect ratio fiber suspensions', *Ph.D. Thesis*, University of Delaware, 1992.
38. H. Kardestuncer and D. H. Norrie, *Finite Element Handbook*, McGraw-Hill, New York, 1987.
39. A. Einstein, 'Eine neue Bestimmung der Moleküldimensionen', *Ann. Phys. (Lpz.)*, **19**, 289–306 (1906).
40. K. C. Nunan and J. B. Keller, 'Effective viscosity of a periodic suspension', *J. Fluid Mech.*, **142**, 269–287 (1984).
41. J. F. Brady and G. Bossis, 'The rheology of concentrated suspensions of spheres in simple shear flow by numerical simulation', *J. Fluid Mech.*, **155**, 105–129 (1985).
42. G. B. Jeffery, 'The motion of ellipsoidal particles immersed in viscous fluid', *Proc. R. Soc. A*, **102**, 161–179 (1922).
43. S. G. Advani and C. L. Tucker III, 'The use of tensors to describe and predict fiber orientation in short fiber composites', *J. Rheol.*, **31**, 751–784 (1987).
44. E. J. Hinch and L. G. Leal, 'The effect of Brownian motion on the rheological properties of a suspension of non-spherical particles', *J. fluid Mech.*, **52**, 683–712 (1972).
45. C. L. Tucker III, 'Flow regimes for fiber suspensions in narrow gaps', *JNNFM*, **39**, 239–268 (1990).
46. H. L. Goldsmith and S. G. Mason, 'The microbiology of dispersions', in F. R. Eirich (ed.), *Rheology: Theory and Applications*, Vol. 4, 1967, pp. 85–250.
47. J. M. Burgers, 'On the motion of small particles of elongated form suspended in a viscous fluid', *Kon. Ned. Akad. Wet.*, **16**, 113–184 (1938).
48. J. B. Harris and J. F. T. Pittman, 'Equivalent ellipsoidal axis ratios of slender rod-like particles', *J. Colloid Interface Sci.*, **50**, 280–282 (1975).
49. R. G. Cox, 'The motion of long slender bodies in a viscous fluid. Part 2. Shear flow', *J. Fluid Mech.*, **45**, 625–657 (1970).
50. A. S. Sangani and A. Acrivos, 'Slow flow past periodic arrays of cylinders with application to heat transfer', *Int. J. Multiphase Flow*, **8**, 193–206 (1982).
51. J. E. Drummond and M. I. Tahir, 'Laminar viscous flow through regular arrays of parallel solid cylinders', *Int. J. Multiphase Flow*, **10**, 515–540 (1984).
52. M. V. Bruschke and S. G. Advani, 'A finite element/control volume approach to mold filling in anisotropic porous media', *Polym. Compos.*, **11**, 398–405 (1990).